SAND96-1789C

This work was supported by the United States Department of Energy under Contract DE-AC04-94AL85000.
Sandia ia a multiprogram laboratory operated by Sandia Corporation, a Lockheed Martin Company, for the United States Department of Energy.

SAND--96-1789C

CONF-9611104--1

Salt-Saturated Concrete Strength and Permeability

T.W. Pfeifle[1], ASCE Member
F.D. Hansen[2], ASCE Member
M. K. Knowles[2], ASCE Member

Abstract

Laboratory-scale experiments applicable to the use of salt-saturated concrete as a seal material for a transuranic waste repository have been completed. Nitrogen gas permeability measurements were made using a flexible-wall permeameter, a confining pressure of 1 MPa, and gas pressure gradients ranging from 0.3 MPa to 0.75 MPa. Results show that salt-saturated concrete has very low intrinsic permeability with values ranging from 9.4×10^{-22} m^2 to 9.7×10^{-17} m^2. Strength and deformation characteristics were investigated under conditions of triaxial compression with confining pressures ranging from 0 to 15 MPa using either axial strain-rate or axial stress-rate control and show that the failure strength of concrete increases with confining pressure which can be adequately described through pressure-sensitive failure criteria. Axial, radial, and volumetric strains were also measured during each test and these data were used to determine elastic properties. Experimental results are applicable in the design and analysis of seal-related functions and apply to other concrete structures subjected to compressive loadings such as dams and prestressed structural members.

Introduction

The U.S. Department of Energy (DOE) plans to dispose of transuranic wastes at the Waste Isolation Pilot Plant (WIPP). The WIPP, located in southeastern New Mexico, is designed to be a full-scale, mined geologic repository. The WIPP underground facility is located in the bedded salt of the Salado Formation at a depth of about 655 m below ground surface. Access to the facility is provided through four vertical shafts. Because the shafts comprise direct communication between lithologic units and connect the repository to the surface, they will be sealed to limit the release

[1]RE/SPEC Inc., P.O. Box 725, Rapid City, South Dakota 57709.

[2]Sandia National Laboratories, P.O. Box 5800, Albuquerque, New Mexico 87185.

DISCLAIMER

of hazardous waste from the repository and to limit groundwater flow into the facility.

The primary engineering guidelines for the shaft seal system state that seal materials should exhibit physical, chemical, and mechanical compatibility with the host salt rock, and have low gas or liquid permeability. Standard concretes possess some of these characteristics. However, the need to construct seals in a salt formation and stringent regulatory requirements provide the impetus to develop specially formulated salt-saturated concretes for the WIPP. Salt-saturated concrete bonds tightly with the halite country rock, thereby preventing channeling of fluid around the seals. Salt-saturated concrete mixes are achieved by the addition of dry salt aggregate or brine.

Candidate concretes developed specifically for WIPP applications include expansive salt-saturated concrete (ESC) [Wakeley and Walley, 1986], and the volumetrically stable Salado Mass concrete (SMC) [Wakeley et al., 1994]. Volume stability of the concretes ensure that the aperture at the shaft concrete/salt interface is minimal. The SMC is currently proposed as a seal material for WIPP shaft seal components.

The salt-saturated concretes developed for WIPP must be evaluated pursuant to the guidelines, which require consideration of the structural and hydrological properties of the material. Structural and hydrological performance evaluations require knowledge of material strength, and elastic moduli and intrinsic permeability, respectively. Strength of portland cement concrete under combined loading has been evaluated previously. Tests have been performed using prismatic specimens with loads applied to the three opposed faces using specially designed bearing platens [e.g., Kupfer et al., 1969; Robinson, 1967]. Other investigators including Richart et al., [1928] and Fumagalli [1965] used cylindrical specimens loaded incrementally in the axial direction to failure, while a constant radial stress is applied using hydraulic fluid. Hollow cylinders subjected either to torsion and axial compression or internal hydraulic pressure and axial compression have been used [e.g., Bresler and Pister, 1958; McHenry and Karni, 1958]. In general, the results of these experiments indicate concrete strength is pressure-sensitive. Although the literature contains numerous references for confined strength of standard concretes, similar information does not exist for salt-saturated concretes.

The strength and deformation properties of the salt-saturated concretes and their pressure sensitivity are important to determine seal adequacy at the WIPP. Compressive stress states will be induced in the seals as the salt creeps inward toward excavated openings. Compressive loads will increase until the original lithostatic stress (approximately 15 MPa) is reestablished in the salt; however, loading of the concrete seals is not expected to be uniform, particularly if the concrete plug is horizontal. Relatively large shear stresses may be induced under certain conditions.

Fluid flow through seal materials depends directly on the intrinsic permeability of the material. Reported permeability values of cementitious sealants range from 10^{-14}

to 10^{-20} m^2 [Lutenegger and DeGroot, 1993]. Field measurements have produced an estimated permeability of 10^{-17} to 10^{-21} m^2 for Small Scale Seal Performance Tests (SSSPT) conducted at the WIPP from 1985 to 1995 [Knowles and Howard, 1996]. The SSSPT used ESC as a sealing material. No permeability tests have previously been conducted on SMC.

This paper presents results of permeability and compression experiments conducted on specimens of salt-saturated concrete prepared from (1) SMC specimens, (2) concrete cores recovered from a commercial salt mine shaft seal, and (3) ESC cores recovered from the SSSPT. In the first experiment, permeability measurements were made on solid, cylindrical specimens subjected to pressure gradients ranging from 0.3 MPa to 0.75 MPa. The tests were performed using nitrogen gas and a flexible-wall permeameter with a confining pressure of 1 MPa. In the second experiment, cylindrical specimens were loaded to failure both in uniaxial compression and triaxial compression with confining pressures to 15 MPa. Uniaxial tests were conducted in axial-strain control at a rate of 1×10^{-5} s^{-1}, while the confined tests were performed at an axial stress rate of 0.3 MPa s^{-1}. The failure data are fitted by two well-known failure criteria, namely Drucker-Prager and Mohr-Coulomb. Elastic moduli including Young's modulus, E, and Poisson's ratio, ν, were determined from each test.

Test Specimens

Cylindrical test specimens were prepared from three salt-saturated concretes described below:

SMC — Salado mass concrete has been tailored for use as a seal component in the WIPP shafts. The SMC mix comprises API Class H portland cement, Class F fly ash, shrinkage-compensating cement, fine silica sand and coarse chert aggregate, and salt. The water/cement ratio for the mix was 0.36. These samples were cast during trial mixtures of mass concrete and stored for 3 years in a brine bath.

MSC Shaft Concrete — Cores of salt-saturated concrete were recovered from a seal being placed in a commercial salt mine shaft. Two mixtures labeled MSC(1) and MSC(2) were used in construction. MSC(1) concrete comprised a typical 27.6 MPa (4,000 psi) design using coarse and sand aggregate and Type I/II cement. The water was salt-saturated in a mix truck before solid components were added. MSC(2) concrete comprised a sand/cement mix that was placed by tremie line under 70 m of water. Granular salt was added to this batch to form brine during mixing.

SSSPT Concrete — Cores of salt-saturated concrete were recovered from the SSSPT in situ experiments that began at the WIPP in 1985. Following retesting in 1995, the SSSPTs were decomissioned and salt-saturated concrete cores became available for this study.

During specimen preparation, SMC and SSSPT samples were cored using a rock mechanics core barrel and brine as a coolant and recirculation agent. The subcores

were cut to approximate length and their ends ground flat and parallel in a surface grinder so that capping was not required. The MSC concrete cores were used as received except their ends were also ground. All test specimens had a nominal length-to-diameter ratio of 2 with nominal diameters of 100 mm for the SMC and SSSPT specimens and 50 mm for the MSC specimens.

Optical petrographic thin sections were prepared from end fragments of SMC and MSC concretes removed during the specimen preparation procedure. Each plug was impregnated with red dye to highlight connected porosity before sectioning. The fine particles of hydrated paste between grains were not differentiated optically; however, flow paths along aggregate surfaces were noted. In general, the red dye imparts a pink hue to the section, indicating that connected permeability was along minute passages within the paste phases. Entrained air vesicles were generally not filled with dye.

Test Equipment and Procedures

Specimen Assembly. Triaxial compression and permeability specimens were placed inside a protective flexible jacket secured to metal platens mounted at either end. The jacket protected the specimen from the hydraulic fluid (silicone oil) used to apply radial stress (confining pressure). Each platen was vented along the central axis to provide access to porous felt metal disks placed in the specimen/platen interfaces. These disks, used only during permeability measurements, ensured one-dimensional flow parallel to the central axis of the specimen.

Permeability Experiment. Jacketed specimens were placed inside the pressure vessel of the testing frame shown in Figure 1 and pressurized to 1 MPa. Hydraulic lines were connected between the bottom platen and a nitrogen-gas reservoir and between the top platen and a manometer vented to the atmosphere. A regulator valve on the nitrogen-gas reservoir was opened to start flow of gas through the specimen and adjusted to induce a nominal gas pressure at the specimen inlet in the range of 0.3 to 0.75 MPa. During a test, measurements of time, confining pressure, axial load, inlet pressure, and change in manometer level were recorded. At least three permeability measurements were performed on each test specimen with the pressure gradient induced across the specimen lowered for each succeeding measurement as recommended by the American Society for Testing and Materials [1989]. Flow rate was determined by performing a linear-least-squares fit to the data comprising the linear portion of the flow-versus-time curve. The flow rates measured for each specimen were plotted as a function of pressure gradient to verify the assumption of laminar flow through the specimen as indicated by a linear relation between flow rate and pressure gradient.

Triaxial Compression Experiment. Two test systems were used to perform the triaxial compression tests on concrete. Confined tests were performed using jacketed specimens and the testing frame depicted in Figure 1. Unconfined tests used unjacketed specimens and a standard MTS 810.15 load frame. Each system and the test procedures are described below in more detail.

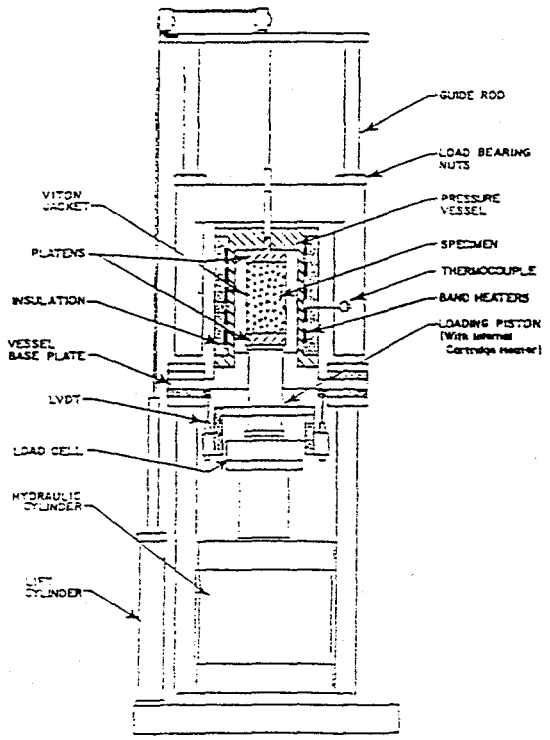

Figure 1. Load Frame Used for Permeability Tests.

In the confined triaxial compression tests, the specimen was first loaded hydrostatically to a pressure of either 5, 10, or 15 MPa. Then the specimen was axially loaded to failure in axial stress control at a rate of 0.3 MPa s^{-1} by advancing the loading piston with the hydraulic cylinder (Figure 1). Confining pressure was maintained at its specified level throughout the test. In the unconfined tests, the specimen was axially loaded to failure at a rate of 1×10^{-5} s^{-1} using the strain control feedback option of the MTS test system. During loading, measurements of axial load, confining pressure (for confined tests), and axial and lateral displacements were made using electronic transducers and a Digital Equipment Corp. LSI 11/23 microprocessor equipped with a 14-bit analog-to-digital converter. Following each test, data reduction software was used to convert measured engineering quantities such as load and displacement to stress and strain using appropriate algorithms and calibration constants. True or logarithmic axial and radial strains were calculated from the initial specimen dimensions and measured axial and radial displacements. True (Cauchy) axial stress was calculated from the axial load and the current cross-sectional area of the specimen as determined from the original specimen diameter and the calculated radial strain.

Test Results

Permeability. Permeability to nitrogen gas was determined using a modified form of Darcy's law which accounts for changes in gas density with pressure; i.e.:

$$k = \frac{2 \mu L Q_e P_e}{A\left(P_i^2 - P_e^2\right)} \qquad (1)$$

where k is the intrinsic permeability (m^2), Q_e is the flow rate at the exit (m^3 s^{-1}), P_e and P_i are the exit and inlet gas pressures respectively (MPa), μ is the viscosity of gas at test temperature (MPa s), L is the specimen length (m), and A is the cross-sectional area of the specimen (m^2). A value of 1.78×10^{-11} MPa s was used for nitrogen viscosity. The flow rate at the exit, Q_e, is the value determined from the least-squares-fit to the data comprising the linear portion of the flow-versus-time curve described earlier. The inlet and exit pressures, P_i and P_e, are absolute

pressures. In this study, the exit pressure is atmospheric or 0.1 MPa and the inlet pressure is the sum of the measured gage pressure and the atmospheric pressure.

Table 1 summarizes all the permeability measurements, while Figure 2 plots permeability as a function of pressure gradient. The results show that the permeability of both the SMC and SSSPT concretes are less than 1×10^{-18} m^2 and that the SMC permeabilities are all less than 1×10^{-20} m^2. The permeabilities of the MSC concrete range between about 1×10^{-17} m^2 and 1×10^{-16} m^2.

Table 1. Results of Permeability Tests on Salt-Saturated Concrete

Concrete	Specimen I.D.	Pressure Gradient (MPa)	Permeability (m^2)
SMC	40SM4-19/2-1/1	0.30	7.5×10^{-21}
		0.30	4.1×10^{-21}
		0.30	4.1×10^{-21}
		0.60	2.1×10^{-21}
		0.75	5.7×10^{-21}
	40SM4-11/2-1/1	0.75	9.4×10^{-22}
SSSPT	MAC313-2/1	0.30	1.0×10^{-19}
		0.30	3.0×10^{-20}
		0.60	5.8×10^{-20}
		0.60	3.5×10^{-19}
		0.75	5.0×10^{-19}
		0.75	4.3×10^{-20}
		0.30	8.0×10^{-20}
		0.60	3.8×10^{-19}
		0.30	4.3×10^{-19}
	MAC314-1/1	0.30	2.3×10^{-19}
		0.30	1.0×10^{-19}
		0.60	2.2×10^{-19}
		0.75	3.1×10^{-19}
MSC	MSC/D-1	0.69	9.7×10^{-17}
		0.50	6.0×10^{-17}
		0.30	4.3×10^{-17}
	MSC/O-2/2	0.69	4.2×10^{-17}
		0.50	2.4×10^{-17}
		0.30	1.8×10^{-17}
	MSC/K-2/2	0.69	3.5×10^{-17}
		0.50	2.6×10^{-17}
		0.30	1.7×10^{-17}

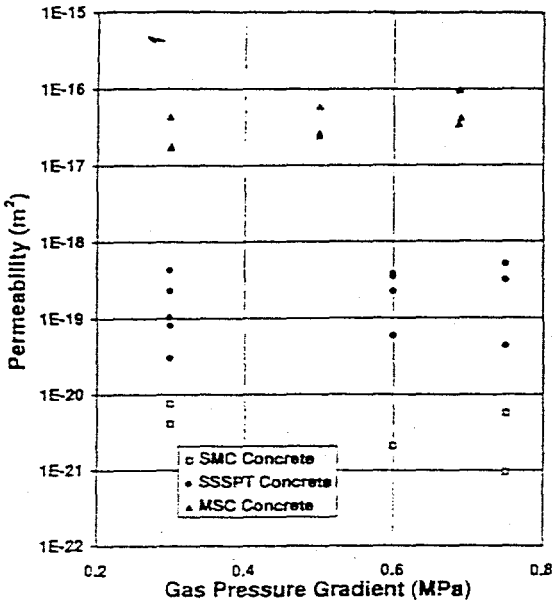

Figure 2. Permeability Versus Gas Pressure Gradient for Salt-Saturated Concrete.

Triaxial Strength. The results of all unconfined and confined triaxial compression strength tests performed on the three types of salt-saturated concrete are summarized in Table 2. In addition to the specimen identification number, values are given for confining pressure, axial stress difference at failure, and elastic moduli calculated over the linear range of the stress-strain curves. Figure 3 plots axial stress difference (i.e., $\sigma_1 - \sigma_3$) as a function of axial and radial strains for each of the four tests performed on SMC concrete. In this figure and throughout this paper, compressive stresses and strains are considered to be positive quantities. The results for SMC show the dramatic increase in strength with confinement. For example, the unconfined strength of SMC concrete is about 45 MPa, while the strength at a confining pressure of 15 MPa is more than 110 MPa.

Table 2. Results of Triaxial Compression Tests on Salt-Saturated Concrete

Specimen I.D.	Confining Pressure (MPa)	Stress Difference at Failure (MPa)	Elastic Moduli	
			Young's Modulus, E (GPa)	Poisson's Ratio, ν
40SM4-19/2-1/1	0	44.2	36.3	0.19
32SM4-25/1-1/1	5	75.8	30.5	0.20
40SM4-11/2-1/1	10	80.5	36.7	0.35
40SM4-2/1-1/1	15	111.4	32.2	0.20
MAC313-2/1	0	74.6	39.1	0.22
MAC313-2/2	5	96.3	37.5	0.35
MAC313-1/1	10	109.7	38.8	0.38
MAC313-1/2	15	116.7	33.2	0.36
MAC314-2/1	0	70.8	42.7	0.22
MAC314-1/1	5	100.8	39.1	0.36
MAC314-2/2	10	109.2	39.8	0.32
MSC/D-1	0	60.2	18.3	0.15
MSC/O-2/2	0	45.3	22.6	0.23
MSC/K-2/2	0	56.4	32.8	0.17

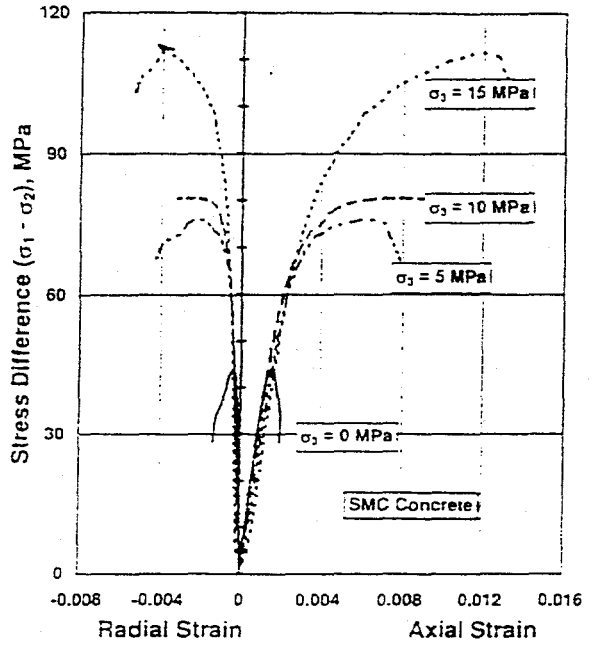

Figure 3. Stress Difference Versus Axial and Radial Strains for SMC Concrete Subjected to Confining Pressures to 15 MPa.

Confining pressure also increases the ductility of the concrete as shown by the increases in the strains at failure (both axial and radial). In contrast, the elastic moduli appear to be affected little by confining pressure. The results of the testing performed on the SSSPT concrete are similar. No confined tests were performed on the MSC concrete, but it is expected that its behavior would be similar to the SMC and SSSPT.

The effect of confining pressure on strength can be quantitatively evaluated by plotting strength and confining pressure in the form of two stress invariants, i.e., the first invariant of the Cauchy stress tensor, I_1, and the second invariant of the deviator stress tensor, J_2. These two invariants are defined as:

$$I_1 = \sigma_1 + \sigma_2 + \sigma_3 \text{ and } \sqrt{J_2} = \left[\frac{1}{6}(\sigma_1 - \sigma_2)^2 + (\sigma_2 - \sigma_3)^2 + (\sigma_3 - \sigma_1)^2\right]^{\frac{1}{2}} \qquad (2)$$

In the triaxial compression test configuration, $\sigma_1 > \sigma_2 = \sigma_3$ so that Equation 2 can be rewritten as:

$$I_1 = \sigma_1 + 2\sigma_2 \quad \text{and} \quad \sqrt{J_2} = \frac{(\sigma_1 - \sigma_3)}{\sqrt{3}} = \frac{\Delta\sigma_1}{\sqrt{3}} \qquad (3)$$

Figure 4 plots the two stress invariants, I_1 and $J_2^{\frac{1}{2}}$, for the failure stress states of SMC and SSSPT concretes and shows that the relationship between the two invariants is nearly linear for both materials. A well-known failure criterion that captures this linear relationship is the Drucker-Prager criterion which can be expressed as:

$$\sqrt{J_2} = \alpha I_1 + k \qquad (4)$$

where α and k are fitting parameters. A linear least squares fit to the data acquired for each type of concrete yields the following relationships:

Drucker-Prager Criterion for SMC	Drucker-Prager Criterion for SSSPT
$\sqrt{J_2} = 0.340 I_1 + 10.90$ (MPa)	$\sqrt{J_2} = 0.298 I_1 + 21.29$ (MPa)

These two models are superposed on the experimental data given in Figure 4 to show how well the models predict the confined strength of both SMC and SSSPT concretes.

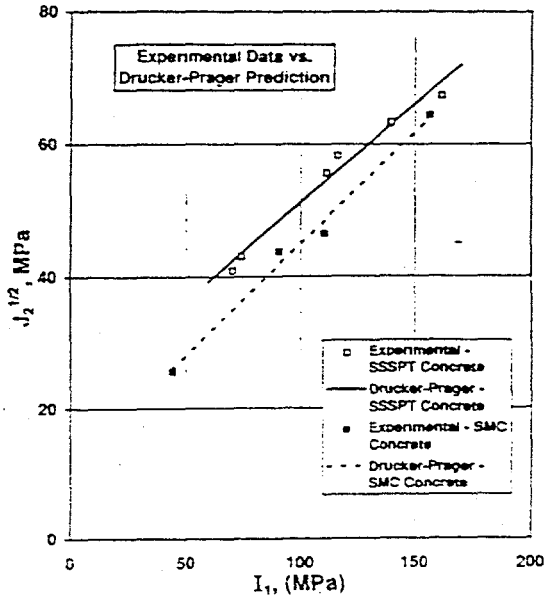

Figure 4. Failure Stress States for Salt-Saturated Concretes.

Another well-known linear failure criterion is the Mohr-Coulomb criterion which for triaxial compression can be expressed as:

$$\sqrt{J_2} = \frac{2\sin\phi}{\sqrt{3}\,(3 - \sin\phi)} I_1 + \frac{2\sqrt{3}\,S_o\cos\phi}{3 - \sin\phi} \qquad (5)$$

where ϕ and S_o are the angle of internal friction and cohesion, respectively. The parameters of the Drucker-Prager and Mohr-Coulomb failure criterion are related in the following manner:

$$\phi = \sin^{-1}\left(\frac{3\alpha\sqrt{3}}{2 + \alpha\sqrt{3}}\right) \quad ; \quad S_o = \frac{(3 - \sin\phi)\,k}{2\sqrt{3}\cos\phi} \qquad (6)$$

Using the fitted values of α and k determined for the SMC and SSSPT concretes, the Mohr-Coulomb parameters were determined from Equation 6 and are $\phi = 43.0°$ and $S_o = 9.97$ MPa for SMC concrete and $\phi = 38.0°$ and $S_o = 18.6$ MPa for SSSPT concrete.

Concluding Remarks

Permeability and triaxial strength of salt-saturated concretes have been measured in the laboratory. Similar to ordinary portland cement concrete, salt-saturated

concrete possesses very low permeability. Strength is pressure sensitive, as expected, and two common failure criteria are fitted to the data. Determination of these properties allows a more thorough analysis of concrete seal structures placed in a natural setting, such as the vertical shafts providing access to the WIPP.

References

ASTM, 1989. "Standard Test Method for Permeability of Rocks by Flowing Air," *Annual Book of ASTM Standards,* Standard D4525, Vol. 4.08.

Bresler, B. and K. Pister, 1958. "Strength of Concrete Under Combined Stresses," *ACI Journal, Proceedings*, Vol. 44, No. 3, pp. 321–345.

Fumagalli, E., 1965. "Strength of Concrete Under Multiaxial Compression," (Caratteristiche de Resistanzia dei Comglomerati Cementizi per Stati di compressione Pluriassiali), *Instituto Sperimentale Modelli e Struture* (Bergamo), Vol. 30.

Knowles, M. K. and C. L. Howard, 1996. "Field and Laboratory Testing of Seal Materials Proposed for the Waste Isolation Pilot Plant," *Waste Management 1996*, Tucson, AZ.

Kupfer, H., H. K. Hilsdorf, and H. Rusch, 1969. "Behavior of Concrete Under Biaxial Stresses," *ACI Journal*, Title No. 66-52.

Lutenegger, A. J. and D. J. DeGroot, 1993. "Hydrologic Properties of Containment Transport Barriers as Borehole Sealants," *Hydraulic Conductivity and Waste Containment Transport in Soils*, ASTM STP 1142, D. E. Daniel and S. J. Trautwein (eds.), ASTM, Philadelphia, PA.

McHenry, D. and J. Karni, 1958. "Strength of Concrete Under Combined Tensile and Compressive Stress," *ACI Journal, Proceedings*, Vol. 54, No. 10, pp. 829–840.

Richart, F. E., A. Brandtzaeg, and R. L. Brown, 1928. "A study of the Failure Mechanism of Concrete Under Combined Stresses," *Bulletin No. 185*, Engineering Experiment Station, University of Illinois.

Robinson, G. S., 1967. "Behavior of Concrete in Biaxial Compression," *Proceedings, ASCE*, Vol. 93, ST1, pp. 71–86.

Wakeley, L. D. and D. M. Walley, 1986. *Development and Field Placement of an Expansive Salt-Saturated Concrete (ESC) for the Waste Isolation Pilot Plant (WIPP)*, Technical Report SL-86-36, U.S. Army Engineer Waterways Experiment Station, Vicksburg, MS.

Wakeley, L. D., J. J. Ernzen, B. D. Neeley, and F. D. Hansen, 1994. *Salado Mass Concrete: Mixture Development and Preliminary Characterization*, SAND93-7066, prepared by Sandia National Laboratories, Albuquerque, NM.